Accepted Manuscript

Title: Low Arsenic Bioaccessibility by fixation in Nanostructured Iron (Hydr)oxides: Quantitative identification of As-bearing phases

Authors: Virginia S.T. Ciminelli, Daphne C. Antônio, Claudia L. Caldeira, Erico T.F. Freitas, Itamar Daniel Delbem, Marcus M. Fernandes, Massimo Gasparon, Jack C. Ng

PII: S0304-3894(18)30189-4
DOI: https://doi.org/10.1016/j.jhazmat.2018.03.037
Reference: HAZMAT 19257

To appear in: *Journal of Hazardous Materials*

Received date: 25-9-2017
Revised date: 28-2-2018
Accepted date: 20-3-2018

Please cite this article as: Ciminelli VST, Antônio DC, Caldeira CL, Freitas ETF, Delbem ID, Fernandes MM, Gasparon M, Ng JC, Low Arsenic Bioaccessibility by fixation in Nanostructured Iron (Hydr)oxides: Quantitative identification of As-bearing phases, *Journal of Hazardous Materials* (2010), https://doi.org/10.1016/j.jhazmat.2018.03.037

Low Arsenic Bioaccessibility by fixation in Nanostructured Iron (Hydr)oxides: quantitative identification of As-bearing phases

Virginia S.T. Ciminelli[a,b]*, Daphne C. Antônio[a], Claudia L. Caldeira [a,b] , Erico, T. F. Freitas[a], Itamar Daniel Delbem[a], Marcus M. Fernandes[d], Massimo Gasparon[b,d], Jack C. Ng[e]

[a]Universidade Federal de Minas Gerais, Belo Horizonte 31270901, Brazil, ciminelli@demet.ufmg.br. Tel: +55 3134091825.

[b]National Institute of Science and Technology on Minerals Resources, Water and Biodiversity, INCT-Acqua, Brazil

[c]Centro de Inovação e Tecnologia SENAI FIEMG – CITSF / Campus CETEC Belo Horizonte 31035536, MG, Brazil,

[d]The University of Queensland, School of Earth and Environmental Sciences, St Lucia 4072, Australia,

[e]The University of Queensland, Queensland Alliance for Environmental Health Sciences (QAEHS), Brisbane 4108, Australia.

*Corresponding author

Graphical abstract

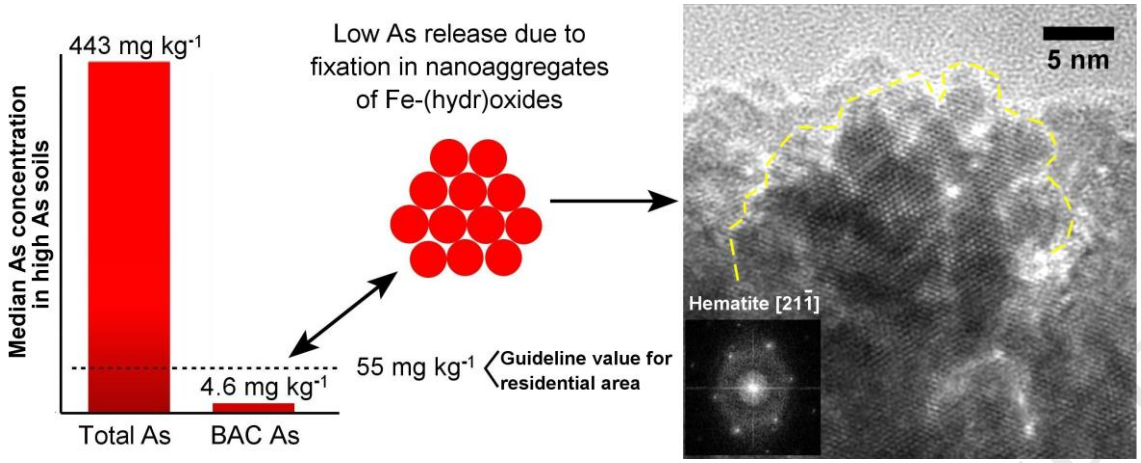

Highlights

- Quantitative, single-particle identification of As-bearing phases in soils
- Phases identified with spatial resolution down to few nanometers
- Arsenic is mainly found in nanostructured, crystalline iron (hydr)oxides
- Arsenic enrichment (up to app. 7,000 mg kg^{-1}) in the coarse fractions
- Low arsenic bioacessibility (0.3 – 5.0%) and low risk to human health

Abstract

A new analytical protocol was developed to provide quantitative, single-particle identification of arsenic in heterogeneous nanoscale mineral phases in soil samples, with a view to establishing its potential risk to human health. Microscopic techniques enabled quantitative, single-particle identification of As-bearing phases in twenty soil samples collected in a gold mining district with arsenic concentrations in range of 8 to 6354 mg kg^{-1}. Arsenic is primarily observed in association with iron (hydr) oxides in fine intergrowth with phyllosilicates. Only small quantities of arsenopyrite and ferric arsenate (likely scorodite) particles, common in the local gold mineralization, were identified (e.g., 7 and 9 out, respectively, of app. 74,000 particles analyzed). Within the high-arsenic subgroup, the arsenic concentrations in the particle size fraction below 250μm ranges from 211 to 4304 mg kg^{-1}. The bioaccessible arsenic in the same size fraction is within 0.86-22 mg

kg^{-1} (0.3-5.0%). Arsenic is trapped in oriented aggregates of crystalline iron (hydr)oxides nanoparticles, and this mechanism accounts for the low As bioaccessibility. The calculated As exposure from soil ingestion is less than 10% of the arsenic Benchmark Dose Lower Limit - $BMDL_{0.5}$. Therefore, the health risk associated with the ingestion of this geogenic material is considered to be low.

Keywords: arsenic fixation in soil, gastric bioaccessibility, nanostructured iron oxy-hydroxides, health-risk assessment, quantitative mineralogy.

1. INTRODUCTION

The stability of As-containing materials in the environment is a concern due to evidence that inorganic arsenic is a human carcinogen [1]. Nonetheless, investigations associating the stability of this element in soil particles and its effect on human health are still scarce, especially in areas influenced by mining activities. Moreover, it remains difficult to establish a clear correlation between the results of extraction tests and the actual stability of As-bearing phases present in soil.

The main source of arsenic in soils is geogenic and therefore related to the parent rock. Background concentrations in natural soil can range from as low as 0.2 mg kg^{-1} to as high as 40 mg kg^{-1} [2], with baseline values generally in the 5–10 mg kg^{-1} range. Nevertheless, arsenic concentrations much higher than the baseline values are found in some mineralized areas and where additional inputs are linked to anthropogenic activities [3]. In soils affected by mining activities, the high concentrations are due to the presence of primary sulfide mineral phases, as well as secondary iron arsenates and iron oxides formed by oxidation of the ore constituents.

The long-term stability of arsenic compounds is a function of several parameters, including site characteristics, particle size and crystallinity, presence/absence of oxygen, complexing agents and on the nature of the As-bearing phases. Dissolution of sulfide

phases, such as arsenopyrite (FeAsS), is favored under acidic, aerated conditions in reactions catalyzed by microbial organisms or under alkaline conditions where chemical reactions predominate. Under reducing conditions, the ferric (hydr)oxides also undergo reduction and dissolution, with the subsequent release of arsenic [4].

The bioavailable and bioacessible arsenic may be significantly lower than the total concentration in a solid matrix, as it represents only the As that is soluble in the body fluids and hence the amount that can be absorbed by the organism. *In vivo* and *in vitro* bioavailability and bioaccessibility tests have become useful tools to determine As exposure from soil ingestion [5]. Arsenic bioavailability can vary markedly with As speciation. Arsenic (V) and As(III) compounds (e.g., Ca ferric arsenate; arsenolite; claudetite; amorphous ferric arsenates) are generally more toxic than arsenic in sulfide minerals (e.g., arsenical pyrite (FeS_2) and arsenopyrite (FeAsS)) [6]. Toujaguez et al. [7] reported bioaccessible As values in mining tailings of up to 35,372 mg kg^{-1} ranging from 0.65 to 40.5% of the total As content, and the difference being related to the mineral phases. A recent study [8] pointed out the importance of the chemical binding type between As and Fe oxide on the bioaccessibility of As in soils. A relatively low bioaccessibility in the co-precipitated sample was attributed to the presence of As within the Fe oxide lattice but unambiguous experimental evidences of the proposed model were not provided.

Soil properties such as pH, aging, the presence of oxides of other elements and total organic carbon (TOC) have been shown to influence bioaccessibility [9,10]. Further, Smith et al. [11] showed an increase in arsenic bioaccessibility with decreasing particle size. Caetano et al. [12] showed arsenic leachability higher for round-shaped scorodite particles than for plate-like shaped scorodite, for particles with the same specific surface area. Therefore, a morphological characterization of As-bearing phases is also relevant.

Precise, single particle characterization of As-bearing phases in environmental samples by traditional analytical techniques is not trivial. Arsenic association with the iron (hydr)oxides (collected or synthesized) is generally explained by models involving inner

sphere complexation or formation of metal arsenates. In line with the adsorption/co-precipitation models, bulk X-ray absorption spectroscopy has helped identify the molecular environment of As in various matrices for more than a decade [6,13,14]. The combination of synchrotron-based techniques with theoretical modeling and other spectroscopic techniques has improved the understanding of the mechanisms of arsenic fixation in typical substrates found in the environment [15]. Micro-X-ray fluorescence combined with microfocused-X-ray absorption spectroscopy has enabled *in situ* characterization of As in soil samples (e.g., oxidation state, association, and coordination) with spatial resolution usually down to the micrometer level [16]. It should be noted that these methods do not provide the spatial resolution necessary to investigate highly heterogeneous nanoscale phases in soil samples, down to a few nanometres, or allow statistically sound quantification of As-bearing phases. To overcome these limitations, we combined high-resolution transmission electron microscopy with scanning electron microscopy and automated image analysis.

This investigation was conducted in a region where elevated arsenic levels associated with gold mineralization are well documented [17]. Gold is found in association with geogenic arsenic anomalies, mainly scorodite ($FeAsO_4.2H_2O$) and arsenopyrite (FeAsS) [18,19]. Gold extraction by artisanal mining dates back to 1734, while industrial mining was established in 1987. There are concerns that the communities living in this mineral-rich region may be exposed to elevated concentrations of As, derived either from the natural weathering and erosion of rocks, and from soils and water, or from mine wastes accumulated over centuries of mining activities. As a result, this region has attracted significant attention from the local and international media over recent years. Within this context, As exposure from soils in this As-enriched environment together with a precise, statistically sound identification of As sources and association is needed. Soil samples were collected and analyzed for bioaccessibility using synthetic gastrointestinal fluids. The bioaccessible As concentrations were used to estimate the daily total As intake from unintentional soil ingestion and then in the assessment of As exposure and the associated risks. Quantitative, single particle identification of As-bearing phases, as well

as their partition and association with other soil constituents, was carried out by using a scanning electron microscopy (SEM)-based automated image analysis system [20]. Nanoscale investigation of As association with the soil constituents was done by Transmission Electron Microscopy (TEM) [21].

The primary aim of this investigation was to develop an analytical protocol for the identification of arsenic in soil samples and for the assessment of its potential risk to human health. It will be demonstrated that the analytical procedure developed by combining statistically sound SEM with automated image analysis with the precise identification of As association by HR-TEM allows the identification of As-bearing nanoparticles in As-rich soils, the form of As association with the soil constituents, and how this association determines As bioaccessibility and potential risks to human health.

2. EXPERIMENTAL

2.1 Sampling, sample preparation and analyses

The soil sampling and analyses were undertaken according to the State Environmental Agency – FEAM [22] protocols and international practice [23]. The sampling was undertaken in four geological units and four classes of soils comprising areas of gold mineralization and areas representing the region's background (Figure 1). The collection of forty-nine surface soil (0-20 cm) samples was carried out in June-July 2014. Twenty-samples were tested for bioaccessibility (fraction <250μm). Based on As concentrations, the samples fell into two groups: high As concentrations (>100 mg kg^{-1}), hereafter labelled "high As" (H-As), and "low As" (L-As) (< 100 mg kg^{-1}).

Figure 1. Sampling location, Paracatu, MG, Brazil, showing the complete set of samples and the selected samples enclosed in square for this study.

The bulk samples were oven-dried at 40ºC for 12 hours then disaggregated, split into sub-samples and sieved at 2 mm, and then finely-ground (<44 μm) for chemical

analyses and particle characterization by TEM.

Energy Dispersive X-ray Fluorescence- EDXRF was carried out in a Shimadzu EDX-7000 energy-dispersive X-ray fluorescence spectrometer to determine total concentrations for major elements. The acid extractable concentration of arsenic in soil samples was determined following digestion with HNO_3/HCl using a microwave-assisted (Ethos, Milestone) digestion procedure [24]. Arsenic was analyzed by inductively coupled plasma optical emission spectrometry (ICP-OES) (Perkin Elmer Optima 7300DV). The digestion and analytical conditions are provided in Tables S1 and S2. Two standard reference materials (NIST SRM 2710a and CANMET/ CCRMP-Till-3) were analyzed together with each batch of 10 samples. Duplicates and analytical blanks were analyzed as well. Arsenic recoveries ranged from 84 to 101% (Tables 1 and S3). All blank extractions returned values below the method detection limits (DL < 0.2 mg L^{-1}). Details on the analytical procedures are provided as Supplementary Material.

2.2 Oral bioaccessibility

The arsenic bioaccessible fraction was determined using the standard operating procedure adopted by the United States Environmental Protection Agency – USEPA [25], which consists of a simple extraction with a glycine solution in an acid environment to simulate the gastric phase (SM). Prior to the test, the < 2 mm soil samples were sieved to < 250 µm. Each batch of extraction experiments consisted in three soils samples performed in triplicate; a blank consisting of a glycine solution at pH 1.5; and a reference soil material (NIST 2710a). A 20 mL aliquot of extracts was then filtered through a 0.45 µm cellulose acetate membrane and stored at 4 ± 2ºC until analysis by hydride generation inductively coupled plasma optical emission spectroscopy (HG-ICPOES); the instrumental conditions are described in Table S4. No statistical differences were observed between samples analysed by HG-ICPOES and ICPMS. Sulfur and Carbon in the soil samples were determined (LECO SC632).

2.3 Electron Microscopy analyses

Six samples representing different soil classes were selected for arsenic-bearing phase characterization and quantitative mineralogy based on single particle using a FEI Quanta 650 Field Emission Gun Scanning Electron Microscope (FEG-SEM) equipped with two Bruker Quantax X-Flash 5010 energy dispersion X-ray (EDX) detectors and FEI's Mineral Liberation Analyzer-MLA suite 3.1.1.283 for data acquisition and process. In this study, the grain-based X-ray mapping (GXMAP) measurement mode was applied to the analyses of polished sections. In this mode, a series of backscattered electron (BSE) images is collected. Identification of mineral grains by MLA is based on BSE image segmentation and collection of EDX-spectra of the particles/grains. Collected EDX-spectra are then classified using a pre-defined list of mineral spectra collected by the user. The method has a resolution of grain size down to 0.1 – 0.2 µm [20]. A summary of the main instrumental parameters is given in Table S5.

For the TEM analyses each powder sample was dispersed in Milli-Q water in Eppendorf tubes and sonicated in ultrasound bath. A drop of each suspension was placed on carbon coated Cu-TEM grids (300 mesh) and left drying in a desiccator. The analysis was performed using High Resolution TEM (HRTEM), Scanning TEM (STEM), EDX spectroscopy and Electron Energy-Loss Spectroscopy (EELS) using a FEI FEG-TEM Tecnai F20 (200 kV).

3. Results and discussion

Four classes of soils are found in areas under the influence of gold mineralization and areas that represent the region's background. Leptosols, which are typically shallow soils over bedrock, thus indicating little influence of pedogenetic process or soil forming processes, occur in the Canastra and Vazante Groups. Ferralsols, which are soils in the advanced state of weathering, are also found in these geological units. Spots of

Fluvisols are found in the Alluvium / Colluvium areas (Figure 1). Chemical analyses of the soil samples indicate medium and high levels of organic matter (7 – 31 g $kg^{-1}C$) [19].

3.1 Bioaccessible arsenic in the soil samples

Table 1 shows the median, mean and range of acid extractable As concentrations for the three size fractions investigated (> 2 mm, < 2 mm and < 250 µm). The size fraction cutoffs were chosen based on national guidelines and USEPA methods [25] for soil classification (< 2 mm) and bioaccessibility test (< 250 µm). Figure 2 shows the acid extractable As concentrations in the three size fractions of H-As samples. The results show relatively high As concentrations in the coarse fraction (> 2 mm), ranging from 1396 to 8036 mg kg^{-1}. For the finer fractions the ranges are 250-6354 mg kg^{-1} and 211 – 4304 mg kg^{-1}, respectively, indicating a decrease in the As concentration with decreasing particle size. The As concentration in the individual samples is shown in Table S3.

Table 1 – Acid extractable (USEPA, 2007) As concentration (mg kg^{-1}) in different size fractions of the selected soils (triplicate) and quality control samples**.**

Figure 2. Concentrations (mg kg^{-1}) of acid extractable (USEPA, 2007) As concentration in the three fractions of the H-As samples. Square dot (in red) represent the median; circle dots, the outliers; the box indicates the 25–75% range of the distribution; and the whiskers represent minimum and maximum.

The concentrations of major elements by EDXRF in different size fractions of the select soil samples are shown in Table S6. The chemical analyses (acid extractable) of iron, aluminum, and arsenic, in the >2mm and < 2 mm size fractions for the H-As samples is provided by Table S7.

The arsenic enrichment in the coarser fractions is likely associated with the iron enrichment (Table S7). The Pearson linear correlation was calculated considering the

combined size fractions. The value of arsenic/iron correlation (H-As samples) of 0.80 corroborates the positive effect of increasing iron concentration on arsenic concentration. The arsenic/Si correlation of -0.65 is consistent with the lack of association of arsenic with the silicate minerals whereas the As/Al correlation of -0.28 is likely a net result of the association of As with iron (hydr)oxides enriched in Al (as it will be shown later) and other Al-containing minerals (e.g. aluminosilicates) free of As.

The H-As samples (Tables 1 and S3) show As concentrations significantly higher than the investigation values [26] for arsenic in soils (< 2 mm) in agricultural (35 mg kg^{-1}) and residential (55 mg kg^{-1}) areas according to Brazilian national criteria. With the exception of sample K36 (47 mg kg^{-1}), all L-As samples show As concentrations below the investigation values for agricultural and residential areas. The investigation value is defined as the concentration of a given substance in soil or in groundwater above which there are potential direct or indirect risks to human health, considering a scenario of standardized exposure [26]. The high As concentrations shown in Table 1 are in agreement with the results available for gold mining regions in the state of Minas Gerais [17,27] and in other parts of the world, such as Australia (81-2270 mg kg^{-1}[28]), England (3.8-848 mg kg^{-1}[29]), the United States (app. 100-1500 mg kg^{-1}[30]) and China (110-802 mg kg^{-1}[31]).

Regarding the soil type (Table S3), Leptosols generally show the highest As concentrations, whereas the Ferralsol and Fluvisol samples have the lowest As levels. Sample K23 is classified as an outlier according the Grubbs' Test (G-test) [32] as it lies at an abnormal distance (>25%) from the mean (Figure 2).

Incidental soil ingestion is the main pathway for As exposure from soils. The < 250 µm fraction is regarded as the one that is likely to stick to hands and hence could result in exposure via hand-to-mouth. Physiologically based extraction test methods have been widely adopted for the estimation of bioavailability, have been validated against *in vivo* models [5] and are accepted by USEPA [25]. Table 2 shows the bioaccessible As concentrations as well as the mean bioaccessible concentration (440 mg kg^{-1}) for NIST

SRM 2710a. The 30 ± 5% BAC agrees with previously reported BAC of 28 ± 17% [33]. The bioaccessible As for the H-As samples varied from 0.86 mg kg^{-1} to 22 mg kg^{-1} with a mean of 7.53 mg kg^{-1} and a median value of 4.60 mg kg^{-1}. The As BAC ranged from 0.3% to 5.0%, with a mean of 1.4% and a median of 0.9%. The relatively large difference between the median and mean values is due to the presence of an outlier (sample K23), and therefore the median values are taken as being more representative. For the L-As samples, BAC varied from 0.22 to 0.69 mg kg^{-1} (0.9% to 6.5%) with mean and median values of 0.4 mg kg^{-1} (2.7% and 2.4%, respectively) (Table 3).

Table 2. Bioaccessible arsenic in the < 250 µm soil samples (n=3) and in the certified material (n=4) (Mean±SD).

The low As BAC for the H-As and L-As samples (means of 1.4% and 2.7%, respectively) found here is consistent with similar finding of other study (2.2%) conducted in the same region [27]. The bioaccessible As (4.6 mg kg^{-1}) indicates that the metalloid is firmly held in the matrix. The arsenic bearing phases and the main features of this association are discussed below.

3.2 Arsenic-Bearing Phases

Table 3 shows the main mineral phases in the soil samples according to the analyses carried out by MLA. The main phases (> 2 wt.%) are quartz (SiO_2), mica/clay minerals, microcline ($KAlSi_3O_8$), goethite and hematite and other non-identified nanoaggregates of Fe-(hydr)oxides. The MLA tool allows for quantitative single particle analysis of large number of grains. The total number of particles ranged from 27,244 (K23 < 2 mm) to 79,330 (K03), which can provide good statistics [34]. The variation in particle counts is due to the selection of a fixed scanning time (2 hours), which results in a larger number of particles per unit area of the polished section in the samples with finer particle size distribution (e.g., K03). Large variations in the content of Fe-(hydr)oxides from approx. 1% (K06) to approx. 45% (K23 (> 2 mm and < 2 mm) and K48 (> 2 mm)) is shown in

Table 3. The mineralogical characteristics of Fe-rich Oxisols developed from mafic rocks in the state of Minas Gerais, Brazil have been recently evaluated [35]. The results show that the Fe content in soils formed in ferriferous environments can be as high as 480.5 g kg^{-1} (or 48% wt). It is important to note that soil samples are usually investigated in particle sizes < 2 mm and therefore the Fe and As enrichment in the coarse fractions, as shown here, may be overlooked. The median Fe content in the H-As for the >2 mm and <2 mm fractions are 16.8% and 5.3 % respectively (Table S7). In general, high iron concentration, and so the Fe (hydr)oxides content, are related to high As concentration. Samples K22, K23 and K48 (Table 3) illustrate this trend. Sample K23, for example, shows the highest As content (approximately 8000 and 6000 mg kg^{-1}, respectively, in the > 2 mm and < 2 mm fractions) and over 40% Fe-(hydr)oxides content in the coarse and fine fractions. In most samples, the total iron (hydr)oxides content (with and without As) varied also with particle size (e.g., sample K48 shows 44% and 11% for > 2 mm and < 2 mm, respectively (Figure 3 (a) and (b)). The high Fe-(hydr)oxides content may explain the As-enrichment in the coarse fractions, as indicated in Figure 1.

The identification and classification of mineral grains according to BSE segmentation and EDX-spectra, confronted with the mineral list pre-defined by the user, implies the matching of unknown phases with specific mineral compositions. The total elemental iron concentrations shown in Table 3 are then the sum of the iron content in each identified mineral phase that contains this element. Table S8 shows that MLA elemental composition (Fe, Si and As) are broadly consistent with the results obtained from bulk chemical analyses. The underestimation of iron in samples K03 and K06 is related to the fine particle size of these samples (approximately 100% below 250 μm by sieving, and approximately 50% of the Fe-(hydr)oxides phases below 4-6 μm, according to MLA imagery) combined with the aggregation of iron oxides with the gangue minerals (Figure S1(a) and (b)). Microscopy methods are typically affected by particle size distribution, shape factors, type of mineral association and others. Therefore, the application of MLA to environmental samples should take these factors into account. A slight bias of

Fe(MLA) to higher numbers, for instance, is expected due to the type of silicates-iron hydroxides association. The fine intergrowth of phyllosilicates with iron hydroxides (Figure 3 (d) and S.1 (c) and (d)) makes it difficult to discern the two phases and this leads to an overestimation of iron minerals. Finally, even though the arsenic concentrations are outside the best range for EDX analyses, the overall trend obtained by MLA is in agreement with the results from the chemical analyses.

Table 4 shows the number of particles of Fe-(hydr)oxides and selected trace mineral phases (< 2 wt.%, and not listed in Table 3) related directly or indirectly to the presence of As in the samples. The presence of trace minerals and their relative importance can be better assessed by the number of identified particles. The arsenopyrite and scorodite are the main arsenic phases in the local sulfide and oxidized ore bodies, respectively. In contrast, arsenic in the soil samples is found mainly in association with Fe-(hydr)oxides, as well as with rare ferric arsenates, likely scorodite, and arsenopyrite. The presence of As in pyrite is not detected (detection limit of app. 0.1 wt%), though pyrite is a potential As carrier [36]. The relatively low number of pyrite particles (8-300) and arsenopyrite (ranging from 0 to 7) is consistent with the low bulk sulfur concentration (median 130 mg kg^{-1}, range of < 100 to 288 mg kg^{-1}), and indicates that the overall contribution of sulfides and arsenates from the mineralized lithologies to the bulk soil chemistry is negligible.

Quantitative automated image analyses are widely used in geometallurgy and mineral processing to identify mineral associations and degree of liberation, among other features. This technique allows the analyses of thousands of particles, which makes it a statistically sound method. The application of the method to soil samples allowed the identification and quantification (which is not trivial) by single-particle analysis of the arsenic association with iron (hydr)oxides as well as with trace constituents, such as arsenopyrite and scorodite. The authors believe that quantification of arsenic-bearing particles brings a relevant and practical contribution to arsenic speciation in the environment.

Table 3. Major mineral phases (wt%) and elemental analyses provided by MLA in selected soil samples

Table 4. Number of particles of selected phases

Figures 3a and 3b show BSE-SEM typical images of polished sections prepared from the soil samples with different iron (hydr)oxides content. Figures 3c and 3d show typical mineral associations found in the soil samples: hematite, quartz, muscovite and the intergrowth of phyllosilicate lamellae with Fe-(hydr)oxides (goethite and hematite). Figures 3e and 3f depict As-bearing, botryoidal goethite and hematite, respectively, both with the typical concentric growth layers that are usually indicative of phase transformation. Fe-(hydr)oxides (Table 3) are the main As reservoir in the soil samples. The intergrowth of phyllosilicates with the Fe-(hydr)oxides should be noted. The low As BAC is consistent with As association with these phases, as they are chemically stable under surficial environmental conditions.

Figure 3. SEM micrographs of typical soil samples: **(a)** (a) K48 > 2mm (27.4% Fe) and (**b)** K48 < 2mm (8.4% Fe), showing the different content of Fe-rich grains (bright) and aluminosilicates (dark) in the coarse and fine fractions; **(c)** (1) Hematite (66.5% Fe, 30.6% O, 1.5% Al, 1.4% As), (2) Quartz, (3) Muscovite; (highlighted by the arrow); **(d)** (4) Muscovite within the Fe-(Hydr)oxide matrix (1.8% As) and (5) Goethite (62.4% Fe, 34.2% O, 1.5% Al, 1.0% As, 0.1% Si, 0.8% P); **(e)** (3) Muscovite, (4) Fe-(Hydr)oxide matrix (1.1% As); (6) Botryoidal goethite (62.9% Fe, 31.9% O, 2.3% Al, 2.9% As); **(f)** (5) Goethite (62.9% Fe, 31.9% O, 2.4% Al, 2.9% As) and (7) Botryoidal hematite (67.0% Fe, 27.8% O, 1.5% Al, 0.6% As, 0.4% Si).

Figure 4 shows typical TEM images of the As-bearing Fe-(hydr)oxides phases. A nanometer-scale map of chemical composition and the spatial distribution of Al, Fe, O and As are provided by STEM-EDS (Fig. 4i-j). The energy dispersive spectroscopy (EDS) maps of Fe-(hydr)oxides aggregates suggest that Al and As are dispersed within the structure of the Fe-(hydr)oxide along with O and Fe. The distribution of As suggests that the metalloid is incorporated in the Fe-(hydr)oxides aggregates. Freitas et al. [21]

investigated As- enriched Fe–Al-oxisols after their use as liners in disposal facilities of sulfide tailings. The results demonstrated that As was present in oriented aggregates formed by crystalline nanoparticles of Fe-(hydr)oxides. The same pattern was found in the samples described in this study. It is important to observe that in the present investigation the samples were collected in sites with no evidence of anthropogenic activities or input from external arsenic sources.

Figure 4. (a) Bright Field TEM image of oriented aggregates (OA) of goethite nanoparticles in K21(< 2mm) and SAED pattern (inset); (b) HRTEM image of white square in (a) Fast Fourier transform (FFT) of goethite; (c-f) EDS maps of goethite(a); (g) Bright Field TEM of K48(> 2mm) showing OA of hematite pointed by arrow; (h) HRTEM image of white square (g) with FFT; (i and j) EDS spectra of goethite(a) and hematite(g). Copper signal from sample grid.

The aggregates shown in Figures 4a and 4g were further investigated by HRTEM analysis. The interplanar distances (*d*) were measured by selected area electron diffraction (SAD) and Fast Fourier Transform (FFT) of the HRTEM image (insets of Figs. 4b and 4h). The d-spaces of goethite reflections (010) and (-401) were measured (inset in Figure 4a). For Figure 4g, the distances of 0.25 nm, 0.27 nm and 0.36 nm correspond to the d_{hkl} of hematite reflections (110), (104) and (102), respectively (Figure 4h). Based on these d_{hkl} spaces, the aggregates were identified as goethite and hematite, respectively. The TEM results demonstrate that the Fe-(hydr)oxides nanoaggregates diffract as a single crystal, as expected for crystals formed by oriented-aggregation crystal growth.

Previous work [16] suggested, according to bulk-XANES spectra, micro-XANES and μ-SXRF analyses, that As occurs mostly in poorly crystalline ferric arsenate with minor arsenopyrite. The low As Bac was ascribed to ferric arsenate, though the less crystalline phase is expected to be relatively soluble [37]. We argue that the low As BAC is a result of As association with crystalline nanoparticles of Fe-(hydr)oxides aggregates. The intergrowth of the Fe-(hydr)oxides with the phyllosilicates adds additional constraint to arsenic release/mobilization as these mineral phases are expected to remain stable.

Arsenic is therefore expected to remain immobilized under a wide range of environmental conditions and therefore pose low risk to human health.

In summary, our work reveals a form of arsenic association with nanoscale iron (hydr)oxides mineral phases in soil samples different from the typical adsorption and co-precipitation phenomena. The association of arsenic with crystalline nanoparticles of iron (hydr)oxides, which is demonstrated to be the predominant fixation mechanism in our soil samples, is not usually explored in the literature. This finding is a unique feature of these, and possibly other, soils.

3.3 Health Risk Assessment and Environmental Implications

The arsenic intake from unintentional ingestion of H-As and L-As soils by adults and children are presented in Table 5 considering three scenarios (A1, A2 and A3). The first one (A1) refers to the median value of BAC for the H-As samples, the second (A2) refers to the maximum BAC As value for the H-As samples and the third (A3) refers to the median value for the L-As soil. The assessment of As exposure was based on the ingestion of 50 mg of soil per day and a body weight of 70 kg for adults, and the ingestion of 100 mg of soil per day and a body weight of 16 kg for children, in line with local regulations [38]. The assessment of exposure was based on the product of exposure factors being equal to 1 (worst-case scenario). Using this very conservative approach, a continuous exposure implies soil ingestion 365 days per year.

Table 5 - Arsenic intake from soil, water and food ingestion and predicted cancer risk.

Risk assessment calculations were carried out by comparing the total As intake to Benchmark Dose Lower Confidence Limit (BMDL) and linear dose relationship for the As Cancer Slope Factors (CSF) for oral ingestion set at 1.5 per mg kg^{-1} b.w.day^{-1}[39]. In Table 5, we illustrate the relative risk in different scenarios of soil ingestion using CSF. The essence of this exercise is to calculate the dietary intake of arsenic and to compare

the results to those of the provisional guideline value of 10 µg L^{-1} in drinking water [40]. It can be noted that when the CSF approach is considered, the soil ingestion in all three scenarios (A1, A2, A3) is one to three orders of magnitude lower (2.4×10^{-5} - 4.5×10^{-7}, respectively) than the risk (4.30×10^{-4}) associated with the ingestion of 10 µg As L^{-1} water. It is worthy to note that even in the most conservative, unlikely scenario (A2) of maximum As BAC and continuous exposure, the calculated risk associated with soil ingestion is lower than that prescribed by WHO for drinking water.

There is an ongoing debate related to the use of CSF and benchmark dose lower limit (BMDL). The derivation of BMDL does not assume that arsenic-induced cancers are non-threshold as the IRIS (Integrated Risk Information System) cancer slope factor does. The inorganic arsenic lower limit on the benchmark dose ($BMDL_{0.5}$) for a 0.5% increased incidence of lung cancer was calculated to be 3 µg kg^{-1} b.w. per day with a margin of exposure (MOE) of approximately 10 (range: 2–7 µg kg^{-1} b.w. per day with MOE of 30 to 1) using a range of assumptions to estimate total dietary exposure to inorganic arsenic from drinking water and food [41]. There is significant evidence from international studies confirming that the BMDL approach adopted by WHO and JECFA [40,41] is more realistic and appropriate than the US EPA linear dose relationship approach for setting the As Cancer Slope Factors (CSF) for oral ingestion and inhalation respectively for risk assessment calculations [39].

The combined risks as well as the contribution of each source of exposure are also calculated for the combined intake of soil, food and water (Table 5). The data for food and water were taken from a recent publication of our group [18] applied to the study region. When water and food intake are taken into consideration, the total intake increases from 0.0033 µg kg^{-1} b.w. day^{-1} (soil only in scenario A1) to 0.1973 µg.kg^{-1} b.w.day^{-1} (soil + water + food) and from 0.0157 µg kg^{-1} b.w. day^{-1} (soil only in scenario A2) to 0.2097 µg kg^{-1} b.w.day^{-1}, with food being the main source of exposure. Under these scenarios, the calculated risks are of the same order of magnitude compared to

that of drinking 10 µg As L^{-1} water. However, the contributions of soil to the total daily As intake remain very low (1.7% for A1 and 7.5% for A2).

The As exposure from soil only or from combined soil, food and water intake is less than 10% of $BMDL_{0.5}$, and therefore we argue that the associated risk to human health for the local population can considered to be low. This conclusion is further supported by the fact that $BMDL_{0.5}$ of 3 µg kg^{-1} b.w. per day (that is, more than an order of magnitude higher than that calculated under the worst-case scenario for the combined soil, food and water intake) has a safety factor of 10 (MOE), which is derived from an epidemiology study conducted on a population exposed to high levels of arsenic and whose nutritional status might have been compromised [41].

4. Conclusions

An analytical protocol was developed to identify arsenic in heterogeneous nanoscale phases in soil samples. The protocol was applied to samples collected in a gold mining district of Minas Gerais, Brazil, during an investigation aimed at establishing the As content and its bioacessibility, the nature of its association with the samples' mineral constituents and the potential risk to human health posed by incidental soil ingestion. Two sets of samples were selected for this study. For the high arsenic (H-As) samples, the median arsenic concentration in the < 250 µm fraction was 443 mg kg^{-1}, with bioaccessible arsenic ranging from 0.86 mg kg^{-1} to 22 mg kg^{-1}(0.3-5% BAC) with a mean of 7.53 mg kg^{-1}(1.4%) and a median value of 4.60 mg kg^{-1}(0.9%). For the low arsenic (median arsenic concentration of 17 mg kg^{-1}) samples (L-As), bioaccessible As ranged between 0.2 and 0.7 mg kg^{-1} (0.9%-6.6%) with mean and median values of 0.44 mg kg^{-1} and 0.42 mg kg^{-1} (2.7% and 2.4%), respectively. Arsenic was mainly found in the iron (hydr) oxides in association with phyllosilicates. High-resolution, transmission electron microscopy demonstrated that arsenic is mainly trapped in oriented aggregates of crystalline iron (hydr)oxide nanoparticles. These findings highlight a new form of arsenic fixation in the environment, usually

described by inner-sphere complexation/co-precipitation models. The calculated As exposure from soil ingestion only, or from a combined soil, food and water intake, was less than 10% of the Benchmark Dose Lower Limit - $BMDL_{0.5}$. Therefore, the risk to human health for the local population from the ingestion of these soils is considered to be low. The form of arsenic in association with the iron (hydr)oxides nanoparticles further substantiates the stability data of As-bearing phases and the low potential risk to human health.

Acknowledgements

The authors are grateful to the Brazilian government agencies – CNPq, FAPEMIG and CAPES, and to Kinross Brasil Mineração (KBM) for financial support and the PVE fellowship from the Science Without Borders program to M. Gasparon. Dr. Lixia Qi at UQ, and Guilhermina Souza, Filipe A. T. Alves and Patricia Lopes at UFMG are gratefully acknowledged for performing the ICP-OES and ICP-MS analyses. The authors also acknowledge the Center of Microscopy/UFMG and the Centre of Microscopy and Microanalysis (UQ).

References

[1] IARC (International Agency for Research on Cancer). Monographs on the Evaluation of Carcinogenic Risks to Humans. IARC Monographs, Volume 100 (C). International Agency for Research on Cancer, Lyon, France. 2012.

[2] WHO Air Quality Guidelines for Europe. Second Edition, 273 p, 2000.

[3] P.L. Smedley, D.G. Kinniburgh, A review of the source, behaviour and distribution of arsenic in natural waters. Applied Geochemistry, vol. 17, (2002), pp. 517-568.

[4] V.S.T. Ciminelli, Arsenic in mining: sources and stability In: 5th International Congress on Arsenic in the Environment - As 2014, Buenos Aires. One Century of the Discovery of Arsenicosis in Latin America (1914-2014). London: Taylor & Francis Group, 2014, pp. 3-7.

[5] J.C. Ng, A. Juhasz, E. Smith, R. Naidu, Assessing the bioavailability and bioaccessibility of metals and metalloids, Environ Sci Pollut Res (2015) 22:8802–8825, DOI 10.1007/s11356-013-1820-9.

[6] G. Brown, A.L. Foster, J. D. Ostergren, Mineral surfaces and Bioavailability of heavy metals: a molecular-scale perspective, Proc. Natl. Acad. Sci. USA. 96, 1999, pp.3388-3395.

[7] R. Toujaguez , F.B. Ono, V. Martins, P.P. Cabrera, A.V. Blanco, J. Bundschuh, L.R.G. Guilherme, Arsenic bioaccessibility in gold mine tailings of Delita, Cuba. Journal of Hazardous Materials, vol. 262 (2013) 1004-1013.

[8] S. Jeong, K. Yang, E. H. Jho, K. Nam. Importance of chemical binding type between As and iron-oxide on bioaccessibility in soil: Test with synthesized two-line ferrihydrite. Journal of Hazardous Materials 330 (2013) 157–164.

[9] Q. Xia, C. Peng, D. Lamb, M. Mallavarapu, R. Naidu, J.C. Ng, Bioaccessibility of arsenic and cadmium assessed for in vitro bioaccessibility in spiked soils and their interaction during the Unified BARGE Method (UBM) extraction. Chemosphere, 147 (2016) 444-450.

[10] Q. Xia, C. Peng, D. Lamb, J.C. Ng, Interaction effects of As, Cd and Pb on their respective bioaccessibility with time in co-contaminated soils assessed by the Unified BARGE Method. Environ Sci Poll. Res., 24 (2017) 5585-5594.

[11] E. Smith, J. Weber, A.L. Juhasz, Arsenic distribution and bioaccessibility across particle fractions in historically soils. Environmental Geochemistry and Health, 31 (2009) 85−92.

[12] M.L. Caetano, V.S.T. Ciminelli, S.D.F. Rocha, M.C. Spitale, C.L. Caldeira, Batch and Continuous Precipitation of Scorodite from Diluted Industrial Solutions. Hydrometallurgy, 95 (2009) 44-52.

[13] A.L. Foster, G.E Brown, T.N. Tingle, G.A. Parks, Quantitative As speciation in mine tailings using X-ray absorption spectroscopy. American Mineralogist, 83 (1998) 553-568.

[14] A.C.Q. Ladeira, V.S.T. Ciminelli, M.C.M. Alves, H.A. Duarte, Mechanism of anion retention from EXAFS and Density Functional Calculations: Arsenic (V) adsorbed on Gibbsite. Geochim. and Cosmochim. Act., 65 (2001) 1211-1217.

[15] G. Duarte, V.S.T. Ciminelli, M.S.S. Dantas, H.A. Duarte, I.F. Vasconcelos, A. F. Oliveira, K. Osseo-Asare, As(III) immobilization on gibbsite: Investigation of the complexation mechanism by combining EXAFS analyses and DFT calculations. Geochimica et Cosmochimica Acta, 83 (2012) 205-216.

[16] F.B. Ono, R. Tappero, D. Sparks, L.R.G. Guilherme, Investigation of arsenic species in tailings and windblown dust from a gold mining area. Environmental Science and Pollution Research, 23 (2015) 638-647.

[17] J.W.V. Mello, W.R. Roy, J.L. Talbott, J. Scott, J.W. Stucki, Mineralogy and arsenic mobility in arsenic-rich Brazilian soils and sediments. Journal of Soils and Sediments, 6 (2006) 9–19.

[18] V.S.T. Ciminelli, M. Gasparon, J.C. Ng, G.C. Silva, C.L. Caldeira, Dietary arsenic exposure in Brazil: The contribution of rice and beans. Chemosphere, 168 (2017) 996-1003.

[19] SENAI/FIEMG -Serviço Nacional de Aprendizagem Industrial. Assessment of Soil Qality in the Ribeirão Santa Rita and Córrego Rico watershed (*in portuguese*). 125 p. 2014. (report)

[20] Y. Gu, Automated scanning electron microscope based mineral liberation analysis. Journal of Minerals and Materials Characterization and Engineering, 2 (2003) 33-41.

[21] E.T.F. Freitas, L.A. Montoro, M. Gasparon, V.S.T. Ciminelli, Natural attenuation of arsenic in the environment by immobilization in nanostructured hematite. Chemosphere 138 (2015) 340-347.

[22] FEAM. Manual of soil collection for reference values of quality in the state of Minas Gerais. (*in portuguese*) 19p, 2013.

[23] USEPA. Preparation of soil sampling protocols: sampling techniques and strategies. 169p, 1992.
[24] USEPA Microwave assisted acid digestion of sediments, sludges, soils and oils - Method 3051a. Revision 1,30p, 2007.
[25] USEPA Standard operating procedure: *in vitro* method for determination of lead and arsenic bioaccessibility. 16p, 2012.
[26] Anonymous CONAMA 420/2009 - CONAMA – CONSELHO NACIONAL DO MEIO AMBIENTE – Resolution no. 420/2009, of December 28, 2009. Provides criteria and guiding values of soil quality for the presence of chemical substances and establishes guidelines for the environmental management of areas contaminated by these substances as a result of anthropic activities. Brasilia DF. (*in portuguese*)
[27] F.B. Ono, L.R.G. Guilherme, E.S. Penido, G.S. Carvalho, B. Hale, R. Toujaguez, J. Bundschuh, Arsenic bioaccessibility in a gold mining area: a health risk assessment for children. Environmental Geochemistry Health, 34 (2012) 457-465.
[28] A.L. Juhasz, P. Herde, C. Herde, J. Boland, E. Smith, Predicting Arsenic Relative Bioavailability Using Multiple in Vitro Assays: Validation of in Vivo-in Vitro Correlations. Environmental Science and Technology, 49 (2015) 11167-11175.
[29] B. Palumbo-Roe, J. Wragg, M. Cave, Linking selective chemical extraction of iron oxyhydroxides to arsenic bioaccessibility in soil. Environmental Pollution 207 (2015) 256-265.
[30] P. Gonzales, O. Felix, C. Alexander, E. Lutz, W. Ela, A. Eduardo Sáez, Laboratory dust generation and size-dependent characterization of metal and metalloid-contaminated mine tailings deposits. Journal of hazardous Materials, 280 (2014) 619-626.
[31] N. Yin, H. Du, Z. Zhang, X. Cai, Z. Li, G. Sun, Y. Cui, (2016). Variability of arsenic bioaccessibility and metabolism in soils by human gut microbiota using different in vitro methods combined with SHIME. Science of the Total Environment, vol. 566-567, pp. 1670-1677.
[32] ISO 5725 (1994) Precision of test methods.
[33] I. Koch, S. Sylvester, V.W.-M. Lai, A. Owen, K. J. Reimer, W. R. Cullen. Bioaccessibility and excretion of arsenic in Niu Huang Jie Du Pian pills. Toxicology and Applied Pharmacology 222 (2007) 357–364.
[34] I.D. Delbem, R. Galéry, P.R.G. Brandão, A.E.C. Peres, Semi-automated iron ore characterisation based on optical microscope analysis: Quartz/resin classification. Minerals Engineering 82 (2015) 2-13.
[35] D.L. Camelo, J. C. Ker, M.P.F. Fontes, M. M. Correa, A.C.S. Costa, V.F. Melo, Pedogenic Iron Oxides in Iron-Rich Oxisols Developed from Mafic Rocks, Rev. Bras. Ciênc. Solo, v.41, 2017. (http://dx.doi.org/10.1590/18069657rbcs20160379)
[36] K.M. Campbell, D.K. Nordstrom, Arsenic speciation and sorption in natural environments. Reviews in Mineralogy & Geochemistry, v.79, 2014, pp. 185-216.
[37] E. Krause, V. A. Ettel, Solubility and stabilities of ferric arsenate compounds. Hydrometallurgy, 22 (1989) 311-337.
[38] Ministry of Health. Guidelines for Evaluation of Risks to Human Health from Exposure to Chemical Contaminants, 2010. (*in portuguese*). http://www.saude.rs.gov.br/upload/1347884770_Avaliacao%20de%20Risco%20-%20Diretrizes.pdf (accessed 02.17.17).
[39] USEPA. Integrated Risk Information System (IRIS) National Center for Environmental Assessment. Arsenic, inorganic (CASRN-7440-38-2), 1995. https://cfpub.epa.gov/ncea/iris/iris_documents/documents/subst/0278_summary.pdf, (accessed 02.17. 17).
[40] WHO Arsenic in drinking-water – Background document for development of WHO guidelines for drinking-water quality. Rev 1, 24 p, 2011.
[41] JECFA (Joint FAO/WHO Expert Committee on Food Additives) (2011). Evaluation of Certain Contaminants in Food. The seventy-second report, WHO, pp. 1-115, 2011

List of Figures

Figure 1. Sampling location, Paracatu, MG, Brazil, showing the complete set of samples and the selected samples enclosed in square for this study.

Figure 2. Concentrations (mg kg^{-1}) of acid extractable (USEPA, 2007) As concentration in the three fractions of the H-As samples. Square dot (in red) represent the median; circle dots, the outliers; the box indicates the 25–75% range of the distribution; and the whiskers represent minimum and maximum.

Figure 3. SEM micrographs of typical soil samples: **(a)** (a) K48 > 2mm (27.4% Fe) and (**b)** K48 < 2mm (8.4% Fe), showing the different content of Fe-rich grains (bright) and aluminosilicates (dark) in the coarse and fine fractions; **(c)** (1) Hematite (66.5% Fe, 30.6% O, 1.5% Al, 1.4% As), (2) Quartz, (3) Muscovite; (highlighted by the arrow); **(d)** (4) Muscovite within the Fe-(Hydr)oxide matrix (1.8% As) and (5) Goethite (62.4% Fe, 34.2% O, 1.5% Al, 1.0% As, 0.1% Si, 0.8% P); **(e)** (3) Muscovite, (4) Fe (Hydr)oxide matrix (1.1% As); (6) Botryoidal goethite (62.9% Fe, 31.9% O, 2.3% Al, 2.9% As); **(f)** (5) Goethite (62.9% Fe, 31.9% O, 2.4% Al, 2.9% As) and (7) Botryoidal hematite (67.0% Fe, 27.8% O, 1.5% Al, 0.6% As, 0.4% Si).

Figure 4. (a) Bright Field TEM image of oriented aggregates (OA) of goethite nanoparticles in K21(< 2mm) and SAED pattern (inset); (b) HRTEM image of white square in (a) Fast Fourier transform (FFT) of goethite; (c-f) EDS maps of goethite(a); (g) Bright Field TEM of K48(> 2mm) showing OA of hematite pointed by arrow; (h) HRTEM image of white square (g) with FFT; (i and j) EDS spectra of goethite(a) and hematite(g). Copper signal from sample grid.

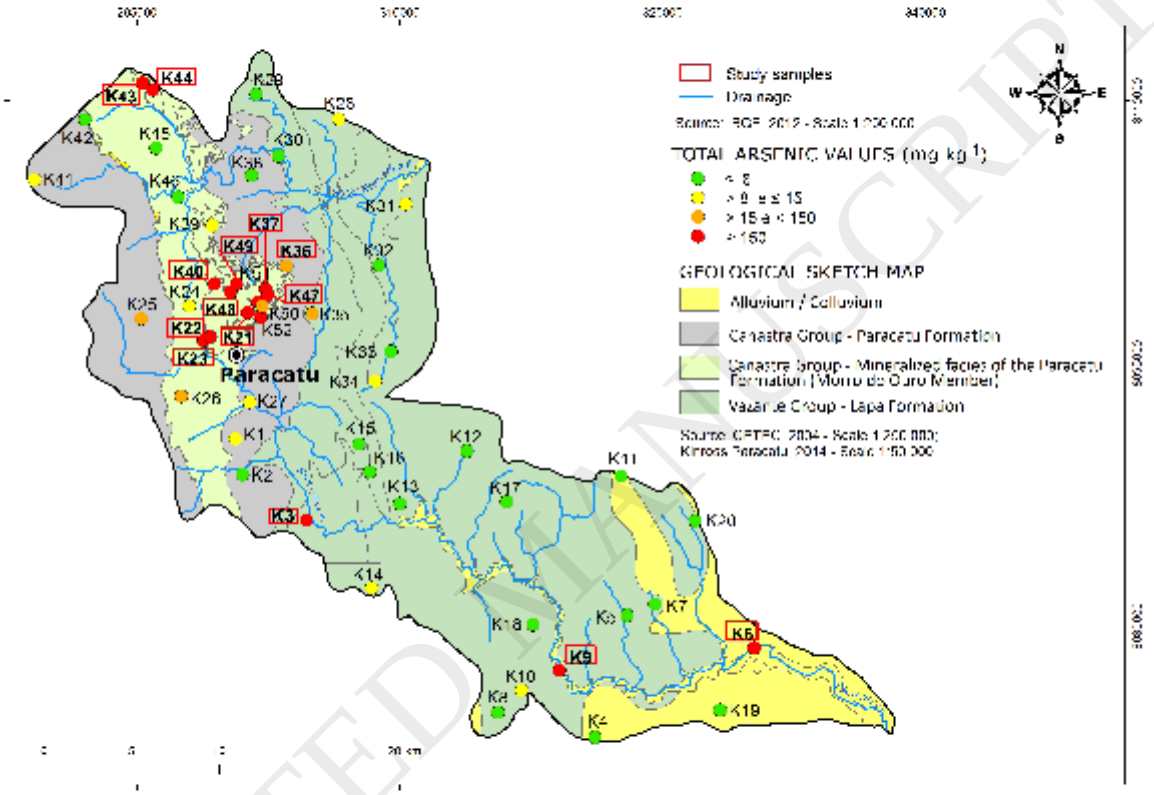

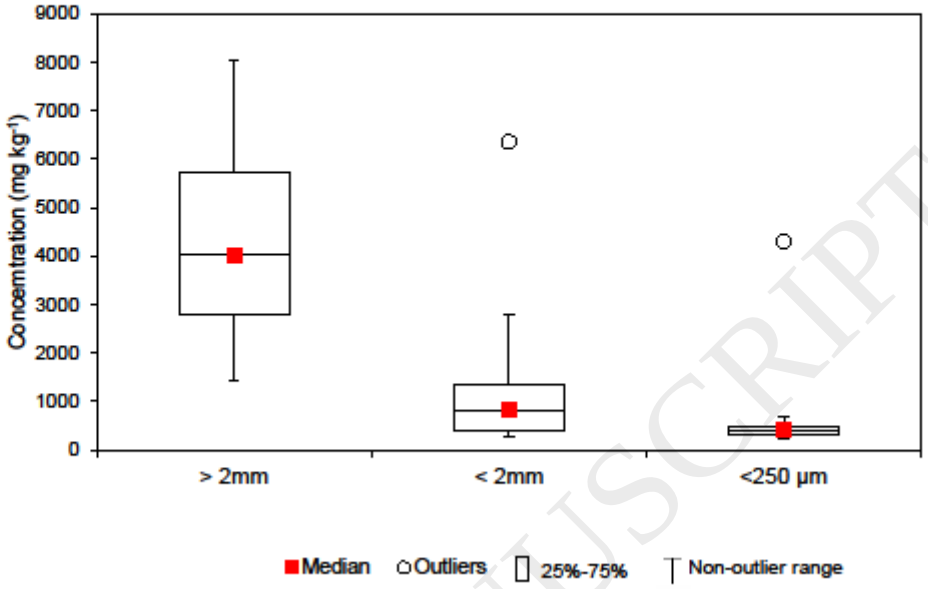

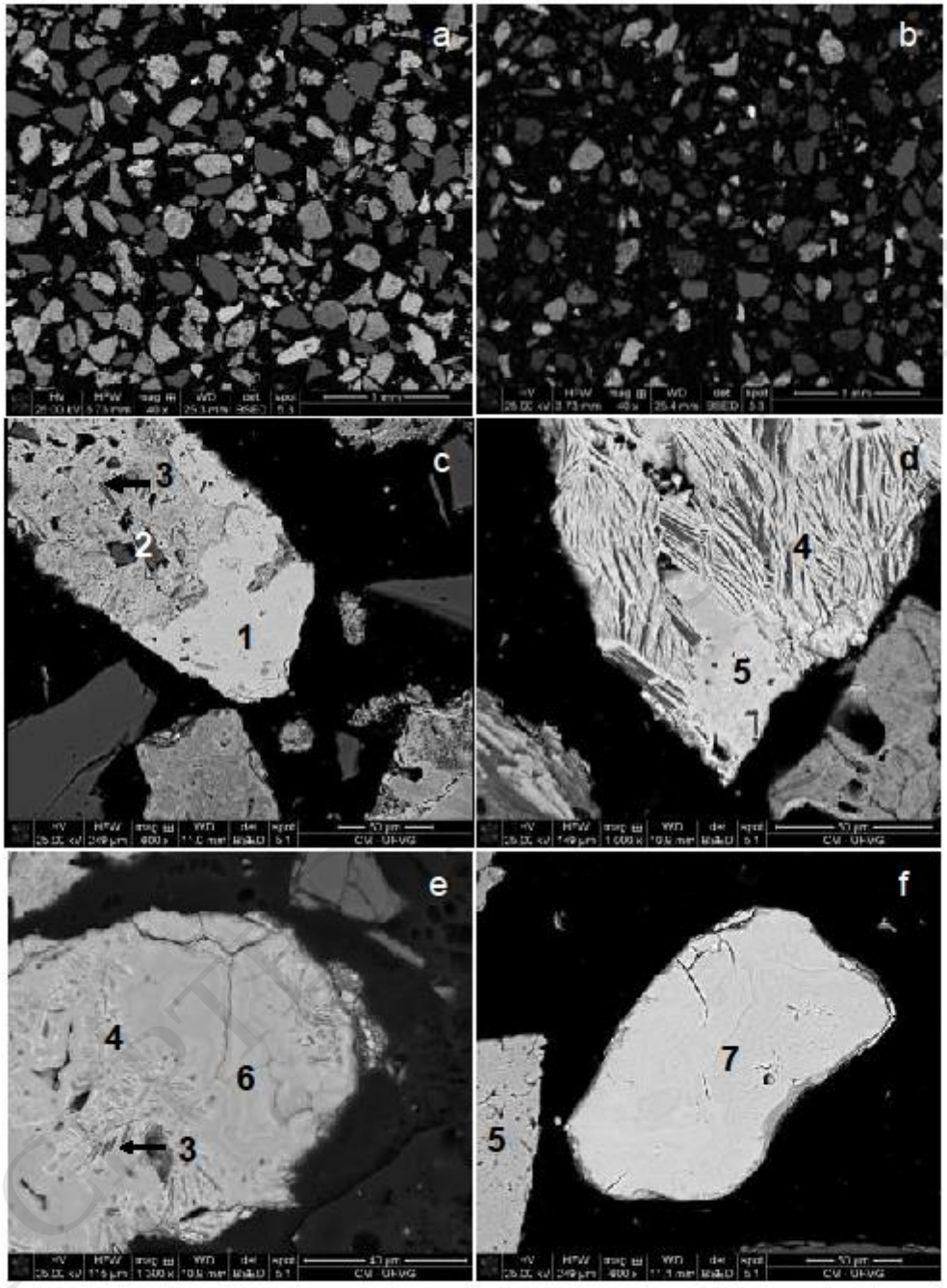

Figure 3

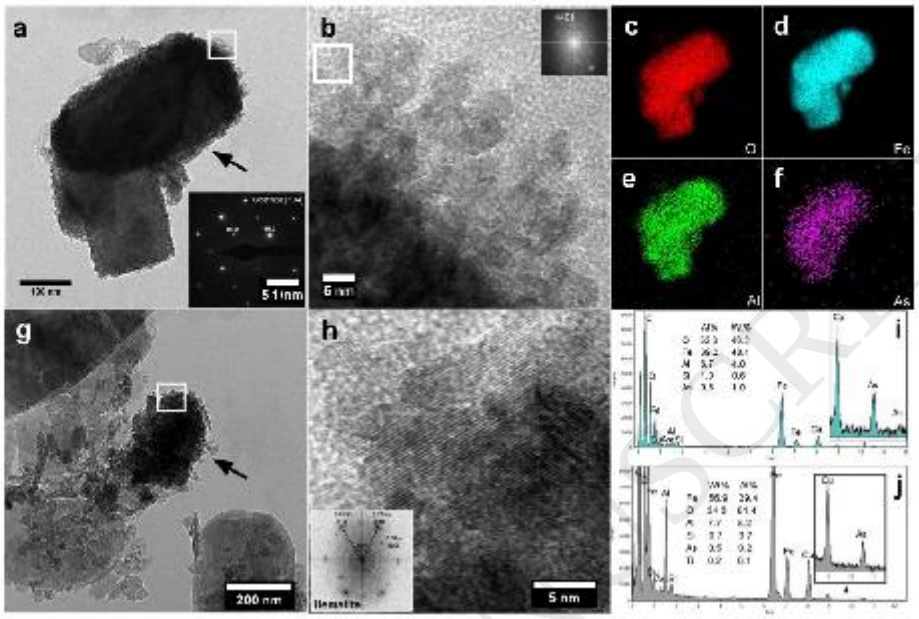

Figure 4.

Table 1 – Acid extractable (USEPA, 2007) arsenic concentration (mg kg^{-1}) in different size fractions of the selected soils (triplicate) and quality control parameters.

	High As concentration (n=13)				Low As concentration (n=7)
	Bulk	> 2mm	< 2 mm	< 250 µm	< 250 µm
Median	1947	4014	806	443	17
Mean	2317	4494	1252	735	22
Range	177-6825	1396-8036	250-6354	211-4304	8-47
SRM NIST 2710a (n=7)		Measured		1557±88	
		Certified value		1540	
		Recovery (%)		101	
RM Till-3 (n=10)		Measured		70±22	
		Certified value		84	
		Recovery (%)		84	

Table 2. Bioaccessible arsenic in the < 250 µm soil samples (n=3) and in the certified material (n=4) (Mean±SD).

Samples	[As] (mg kg^{-1})	Bioaccessible As (mg kg^{-1})	As bioaccessibility (%)
High As samples (H-As)			
K03	464±64	1.9±0.1	0.41±0.03
K06	405±3	1.21±0.01	0.30±0.00
K09	325±5	1.8±0.1	0.57±0.03
K21	841±28	19.47±0.03	2.31±0.00
K22	575±83	1.9±0.4	0.33±0.10
K23	4304±286	17±1	0.39±0.03
K37	494±6	8.2±0.6	1.67±0.10
K40	443±14	22±4	5.01±1.00
K43	211±39	0.86±0.04	0.41±0.02
K44	459±15	4.3±0.9	0.94±0.20
K47	379±33	9.3±2.9	2.45±0.80
K48	324±29	4.6±0.1	1.42±0.05
K49	332±36	5.4±1.3	1.62±0.40
Mean	735	7.53	1.4
Median	443	4.60	0.9
Min.	211	0.86	0.3
Max.	4304	22	5.0
Low As samples (L-As)			
K01	8	0.505±0.004	6.55±0.06
K26	22	0.30±0.02	1.40±0.05
K27	28	0.69±0.05	2.45±0.15
K31	16	0.420±0.004	2.70±0.02
K35	17	0.56±0.06	3.25±0.32
K36	47	0.42±0.01	0.89±0.02
K46	13	0.22±0.02	1.66±0.18
Mean	22	0.44	2.7
Median	17	0.42	2.4
Min.	8	0.22	0.9
Max.	47	0.69	6.5
SRM NIST 2710a			
Indicative value	1540	-	28±17*
Measured (n=4)	1461±41	440±74	30±5

*reported by the literature [33]

Table 3 - Major mineral phases (wt%) in soil samples.

				Samples				
	K03	K06	K21	K22	K23		K48	
	(<2mm)	(<2mm)	(<2mm)	(<2mm)	(>2mm)	(<2mm)	(>2mm)	(<2mm)
Mineral phases	*Composition (%)*							
Fe Oxides/Hydroxides-(no As)	1.7	0.7	1.4	22.5	23.2	19.1	22.6	6.7
Fe Oxides/Hydroxides-As	0.6	0.2	4.1	5.7	20.9	15.7	21.3	4.4
Quartz	21.6	6.2	49.1	24.1	27.1	33.5	26.6	28.2
Ilmenite	----	----	2.7	1.6	----	3.7	----	4.2
Mica/Clay Minerals	67.8	84.1	36.8	43.0	27.2	26.0	27.6	50.7
Microcline	4.3	6.3	3	1.8	----	----	----	4.4
Others ([Wt and Area] <2%)	4	2.5	2.9	1.3	1.6	2.0	1.9	1.4
Total	100.0	100.0	100.0	100.0	100.0	100.0	100.0	100.0
Elemental chemical analyses by MLA (%)								
Fe(Total)	2.2	0.8	4.4	18.2	27.6	22.9	27.4	8.4
Fe(OX-HY)*	1.4	0.5	3.3	17.6	27.2	21.5	27	6.8
Si	26.1	22.9	32	21.2	18.7	21.5	18.6	25.5
As	<0.1	<0.1	0.1	0.1	0.5	0.4	0.5	0.1
Total particle number	79330	73857	41831	49570	32282	50022	33864	59477
*Fe OX/HY = from Fe-(hydr)oxides phases from MLA analyses								

Table 4 - Number of particles identified for selected phases.

				Samples				
Phases	K03	K06	K21	K22	K23		K48	
	(<2mm)	(<2mm)	(<2mm)	(<2mm)	(>2mm)	(<2mm)	(>2mm)	(<2mm)
Fe (hydr)oxides	2765	1880	1453	11483	13654	11268	12914	3161
Fe (hydr)oxides-As	738	396	2901	4776	11822	9459	11702	1968
Pyrite	80	37	287	232	300	102	54	8
Arsenopyrite	0	7	4	0	0	0	0	0
Scorodite*	0	9	1	0	2	2	0	0
Total particle number	79330	73857	41831	36123	32282	27244	33864	59477

*Scorodite composition was well matched but the presence amorphous ferric arsenate cannot be fully discarded.

Table 5 - Arsenic intake from soil, water and food ingestion and predicted cancer risk

Pathway	iAs ingestion (µg per kg b.w.day)		Predict Cancer Risk	% Intake adult (A1)	% Intake adult (A2)
	Adult	Child			
A1 - H-As soils (median As BAC 4.6 mg kg^{-1})	0.0033	0.0288	4.9E-06	1.7	
A2 - H-As soils (max As BAC 22 mg kg^{-1})	0.0157	0.1375	2.4E-05		7.5
A3 - L-As soils (median BAC As 0.42 mg kg^{-1})	0.0003	0.0026	4.5E-07		
B - Food [18]	0.188	0.094	2.8E-04	95.3	89.6
C - Water (0.21 µg L^{-1}) [18]	0.006	0.013	9.0E-06	3.0	2.9
Total (A1, B, C)	0.1973	0.1359	3.0E-04		
Total (A2, B, C)	0.2097	0.2446	3.1E-04		
Total (A3, B, C)	0.1943	0.1099	2.9E-04		
Water (10 µg L^{-1})	0.286	0.625	4.3E-04		